bioRxiv preprint doi: https://doi.org/10.1101/2025.01.10.632426; this version posted January 14, 2025. The copyright holder for this preprint (which was not certified by peer review) is the author/funder, who has granted bioRxiv a license to display the preprint in perpetuity. It is made available under aCC-BY-ND 4.0 International license.

Langerhans Cells Drive Tfh and B Cell Responses Independent of Canonical Cytokine Signals

Aurélie Bouteau[1], Zhen Qin[1], Sandra Zurawski[2,3], Gerard Zurawski[2,3] and Botond Z. Igyártó[1]*

[1]*Department of Microbiology and Immunology, Thomas Jefferson University, Philadelphia, PA 19107, United States.*

[2]*Baylor Scott & White Research Institute, Dallas, TX 75204, United States.*

[3]*Vaccine Research Institute, INSERM, Unité U955, Institut Mondor de Recherche Biomédicale, Créteil, France.*

[*]*Lead/Corresponding author: botond.igyarto@jefferson.edu*

bioRxiv preprint doi: https://doi.org/10.1101/2025.01.10.632426; this version posted January 14, 2025. The copyright holder for this preprint (which was not certified by peer review) is the author/funder, who has granted bioRxiv a license to display the preprint in perpetuity. It is made available under aCC-BY-ND 4.0 International license.

ABSTRACT

Dendritic cells (DCs) are key regulators of adaptive immunity, guiding T helper (Th) cell differentiation through antigen presentation, co-stimulation, and cytokine production. However, in steady-state conditions, certain DC subsets, such as Langerhans cells (LCs), induce T follicular helper (Tfh) cells and B cell responses without inflammatory stimuli. Using multiple mouse models and *in vitro* systems, we investigated the mechanisms underlying steady-state LC-induced adaptive immune responses. We found that LCs drive germinal center Tfh and B cell differentiation and antibody production independently of interleukin-6 (IL-6), type-I interferons, and ICOS ligand (ICOS-L) signaling, which are critical in inflammatory settings. Instead, these responses relied on CD80/CD86-mediated co-stimulation. Our findings challenge the conventional three-signal paradigm by demonstrating that cytokine signaling is dispensable for LC-mediated Tfh and B cell responses in steady-state. These insights provide a framework for understanding homeostatic immunity and the immune system's role in maintaining tolerance or developing autoimmunity under non-inflammatory conditions.

SUMMARY STATEMENT

Langerhans cells (LCs) drive germinal center Tfh and B cell responses in steady-state conditions independently of IL-6, type-I interferons, and ICOS ligand, challenging the established cytokine-centric model of T cell differentiation.

INTRODUCTION

Dendritic cells (DCs) are critical in training and educating naïve T cells and their differentiation into specific T helper subsets (Merad et al., 2013; Yin et al., 2021).

bioRxiv preprint doi: https://doi.org/10.1101/2025.01.10.632426; this version posted January 14, 2025. The copyright holder for this preprint (which was not certified by peer review) is the author/funder, who has granted bioRxiv a license to display the preprint in perpetuity. It is made available under aCC-BY-ND 4.0 International license.

Generally, it is widely accepted that the DCs provide three signals to naïve T cells in the form of cognate peptide/MHC, membrane-bound co-stimulation, and soluble cytokines. Out of these, the cytokines, as third signals (Curtsinger et al., 1999), are regarded as key components in T helper cell differentiation into T helper subsets, such as Th1, Th2, Th17, Tfh cells, and others (Yin et al., 2021; Hilligan and Ronchese, 2020). These distinct Th subsets are thought to be induced by the DC-derived polarizing cytokines specific for each Th subset. The Th polarizing cytokines are induced by exposure to various inflammatory stimuli sensed by DC through distinct pathogen-associated molecular pattern receptors (Janeway and Medzhitov, 2002). This oversimplified model of Th differentiation provides a plausible explanation for inflammatory settings, but it is challenging to apply in a broader sense. For example, antigen targeting to different DC subsets in steady-state in the apparent lack of adjuvant and other inflammatory signals induces Tfh cells and antibody responses (Yao et al., 2015; Bouteau et al., 2019; Caminschi and Shortman, 2012; Kato et al., 2015; Corbett et al., 2005; Li et al., 2015; Lahoud et al., 2011; Kato et al., 2020; Caminschi et al., 2008). Furthermore, anti-commensal responses, termed homeostatic immunity, happen regularly in the absence of overt inflammation (Belkaid and Harrison, 2017), justifying the need to understand better the induction mechanism of adaptive immune responses in this non-inflammatory context.

LCs, with monocytic origin but DC functions (Ginhoux et al., 2006; Hoeffel et al., 2012; Doebel et al., 2017), drive Tfh cells and germinal center (GC)-dependent protective antibody responses in steady-state (Yao et al., 2015; Bouteau et al., 2019). They do this irrespective of the nature of the receptor targeted and without signs of activation and

bioRxiv preprint doi: https://doi.org/10.1101/2025.01.10.632426; this version posted January 14, 2025. The copyright holder for this preprint (which was not certified by peer review) is the author/funder, who has granted bioRxiv a license to display the preprint in perpetuity. It is made available under aCC-BY-ND 4.0 International license.

maturation (Yao et al., 2015; Bouteau et al., 2019). However, the mechanism by which LCs support adaptive immune responses in steady-state remains elusive. Therefore, here, we set out to define the mechanism. We found that LCs induced Tfh and B cell responses independently from IL-6, type-I interferon, and ICOS-L, which were previously reported to play critical roles in inflammatory settings in driving Tfh cells and antibody responses (Crotty, 2014; Krishnaswamy et al., 2018; Crotty, 2019). LC-induced responses, however, were dependent on CD80/CD86 co-stimulation.

RESULTS AND DISCUSSION

LCs, unlike cDC1s, induce GC-Tfh cells and antibody responses in steady-state

We have previously shown using two mouse models that steady-state antigen targeting to LCs, but not cDC1, leads to GC-Tfh formation and antibody responses (Bouteau et al., 2019). In mouse skin, Langerin expression is confined to LCs and $CD103^{+}$/$XCR\text{-}1^{+}$ cDC1s (Kaplan, 2017), and thus, we used two mouse models, huLangerin and $Batf3^{-/-}$ mice, to permit targeting antigen to either LCs or cDC1s. The huLangerin mice express human Langerin specifically in LCs (Bobr et al., 2010), allowing antigen targeting to LCs in the presence of cDC1s using anti-human Langerin (Yao et al., 2015; Bouteau et al., 2019; Igyártó et al., 2011). The $Batf3^{-/-}$ mice lack the migratory Langerin-expressing cDC1s. Therefore, the remaining LCs can be specifically targeted using anti-mouse Langerin (Bouteau et al., 2019; Yao et al., 2015). To further strengthen our previous findings and increase rigor, here, we expanded our toolset to include two other mouse models that were more recently generated by the Murphy lab, XCR1-Cre and $IRF8^{32\Delta}$, both specifically affecting cDC1s (Durai et al., 2019; Ferris et al., 2020). We bred the

bioRxiv preprint doi: https://doi.org/10.1101/2025.01.10.632426; this version posted January 14, 2025. The copyright holder for this preprint (which was not certified by peer review) is the author/funder, who has granted bioRxiv a license to display the preprint in perpetuity. It is made available under aCC-BY-ND 4.0 International license.

XCR-1-Cre to "STOP"-DTA mice to selectively eliminate all the cDC1s (**Fig. 1 A**). The huLangerin-DTA (huL-DTA) mice that lack LCs (Kaplan et al., 2005) were used as controls for cDC1s targeting that does not induce GC-Tfh cells and antibody responses in steady-state (Yao et al., 2015; Bouteau et al., 2019). The mice were then adoptively transferred with CD4 TEα cells and injected with 1 μg of anti-muLangerin-Eα a day later. Four and fourteen days later, the antigen-specific $CD4^+$ T cell and B cell responses were characterized using flow cytometry and ELISA, respectively, as described previously (Yao et al., 2015; Bouteau et al., 2019). We found that LCs targeted in XCR-1-Cre-DTA and $IRF8^{32\Delta}$ mice, like $Batf3^{-/-}$ mice, induced GC-Tfh cells, in sharp contrast to cDC1 targeting in huL-DTA mice (**Fig. 1 B**). The B cell responses mounted in these two new models followed a largely similar trajectory to $Batf3^{-/-}$ mice but were slightly less pronounced (**Fig. 1 C**). Interestingly, the $IRF8^{32\Delta}$ mice did not produce significant levels of antibodies, unlike XCR1-Cre-DTA and $Batf3^{-/-}$ mice (**Fig. 1 D**). This could indicate that this $IRF8^{32\Delta}$ deletion might affect GC and plasma cell responses, as has been reported for full $IRF8^{-/-}$ mice (Carotta et al., 2014; Wang et al., 2019). Thus, these data further support our previous observation that LCs, unlike cDC1s, can induce GC-Tfh cells and antibody responses in steady-state, irrespective of the mouse model used.

Type I interferon is not required for the induction of adaptive immune responses by steady-state LCs

It is unknown how adaptive immune responses, including T follicular helper cells and antibody responses, are induced by LCs and some DC subsets in steady-state. Intact type-I interferon signaling in DCs is needed to effectively induce Tfh cells in

bioRxiv preprint doi: https://doi.org/10.1101/2025.01.10.632426; this version posted January 14, 2025. The copyright holder for this preprint (which was not certified by peer review) is the author/funder, who has granted bioRxiv a license to display the preprint in perpetuity. It is made available under aCC-BY-ND 4.0 International license.

inflammatory settings through IL-6 up-regulation (Cucak et al., 2009). Targeted delivery of IFNα to cDC1 through Langerin enables these cells to support the differentiation of GC-Tfh cells and GC-dependent antibody responses (Bouteau et al., 2019). Based on these data, we hypothesized that steady-state levels of type-I interferon signaling in LCs might play a role in inducing Tfh cells and B cell responses in steady-state. To test this hypothesis, we bred the huLangerinCre mice to IFNαR1$^{f/f}$ mice to delete IFNαR1 from LCs (**Fig. 2 A**). The genotypes of the resulting mice were determined using standard PCR, while the selective deletion of IFNαR1 protein on LCs was confirmed using flow cytometry (**Fig. S1 A**). Cre-positive and cre-negative mice were then adoptively transferred with CD4$^+$ TEα cells and, a day later, were injected with 1 μg of anti-huLangerin-Eα. Four and fourteen days later, the antigen-specific CD4$^+$ T cell and B cell responses were characterized using flow cytometry and ELISA. The anti-huIgG IgG levels were determined using ELISA on serum samples harvested on day 14 (**Fig. 2 A**). We found no major differences regarding antigen-specific CD4$^+$ T cell and B cell expansions and phenotype. The percent of Tfh cells slightly decreased but this was not reflected in the B cell responses. (**Fig. 2, B and C**). The anti-huIgG4 IgG levels were also unaffected without type-I interferon signaling in LCs (**Fig. 2 D**). These data, therefore, point to the lack of a critical role of type-I interferon signaling in LCs in the steady-state induction of Tfh cells and antibody responses.

To increase the rigor of our findings, we used a blocking antibody against IFNαR (**Fig. 2 E** and **Fig. S1 B**), which can address potential type-I interferon involvement in LC-induced adaptive immune responses in steady-state by acting directly on the T cells or indirectly through other cells. Again, we found no significant changes in T and B cell

bioRxiv preprint doi: https://doi.org/10.1101/2025.01.10.632426; this version posted January 14, 2025. The copyright holder for this preprint (which was not certified by peer review) is the author/funder, who has granted bioRxiv a license to display the preprint in perpetuity. It is made available under aCC-BY-ND 4.0 International license.

responses and a moderate increase rather than decrease or absence of anti-hIgG antibody levels (**Fig. 2, F and G**). Thus, these data strongly support that the adaptive immune responses induced by steady-state LCs are largely independent of type-I interferon signaling.

Next, we tested whether exogenous IFNα could boost adaptive immune responses above the levels induced by steady-state LCs. For this, we used an anti-muLangerin-IFNα construct we previously described that enables cDC1 to support antibody responses (Bouteau et al., 2019). LCs, similarly to cDC1, express IFNαR (**Fig. S1 A**). We found that delivering IFNα to LCs did not significantly alter their ability to support B cell responses (**Fig. S1 C**). In total, these data show that either promulgating or diminishing IFNα signaling in LCs does not affect their ability to support adaptive immune responses in this targeting model.

IL-6 is not required for the induction of adaptive immune responses by steady-state LCs

IL-6 in mice, according to some but not all reports, plays a critical role in supporting the differentiation of Tfh cells in inflammatory models (Crotty, 2019). However, its role in Tfh cell and antibody response induction in a steady-state is unknown. Steady-state LCs, unlike cDC1s, contain high levels of IL-6 mRNA transcript (Bouteau et al., 2019). Since LCs, but not cDC1s, can induce Tfh cells with germinal center (GC) phenotype (Bcl-6^{high}) and protective antibody responses in steady-state models (Yao et al., 2015; Bouteau et al., 2019), we hypothesized that LC-derived IL-6 might be essential in supporting the adaptive immune responses. To test this and limit IL-6 deficiency to LCs,

bioRxiv preprint doi: https://doi.org/10.1101/2025.01.10.632426; this version posted January 14, 2025. The copyright holder for this preprint (which was not certified by peer review) is the author/funder, who has granted bioRxiv a license to display the preprint in perpetuity. It is made available under aCC-BY-ND 4.0 International license.

we bred the IL-6$^{f/f}$ mice (Sanchis et al., 2020) to the huLangerinCre mice (Kaplan et al., 2007) (**Fig. 3 A**). The resulting genotypes were determined using PCR, and the selective genomic recombination of the IL-6 locus in LCs was confirmed using PCR on sorted cells (**Fig. S1 D**). We then tested whether LC-derived IL-6 is needed to induce Tfh cells and antibody responses. The mice were transferred with transgenic CD4$^+$ TEα cells and then injected with 1 μg of anti-huLangerin-Eα intraperitoneally, as described above. Cre-negative IL-6$^{f/f}$ littermate mice served as controls. The mice were sacrificed 4 and 14 days later to characterize antigen-specific CD4$^+$ T cell and B cell responses as presented above (**Fig. 3 A**). The expansion and phenotype of TEα cells in the absence of LC-derived IL-6 remained unchanged (**Fig. 3 B**). The B cell responses, including GC cells and anti-hIgG IgG serum levels, showed no significant changes (**Fig. 3 C**). Thus, these data support the idea that LC-derived IL-6 is not required to support steady-state adaptive immune responses.

To rule out the possibility that IL-6 produced and secreted by bystander cells might aid the induction of adaptive immune responses by steady-state IL-6 deficient LCs, we performed IL-6 blocking experiments. Batf3$^{-/-}$ mice were treated with anti-IL-6 or isotype antibodies throughout the experiment (**Fig. 3 D**). Luminex® assay on serum samples was used to confirm the efficiency of IL-6 blockade (**Fig. S1 E**). The antibody-treated Batf3$^{-/-}$ mice that lack cDC1s were adoptively transferred with CD4$^+$ TEα cells and then injected with 1 μg of anti-muLangerin-Eα, and then T and B cell responses were assessed as presented above. We found no significant differences in antigen-specific CD4$^+$ T cell and B cell expansions and phenotype (**Fig. 3, D and F**). The anti-huIgG IgG ELISA on serum samples revealed only a moderate decrease in antibody levels in the

bioRxiv preprint doi: https://doi.org/10.1101/2025.01.10.632426; this version posted January 14, 2025. The copyright holder for this preprint (which was not certified by peer review) is the author/funder, who has granted bioRxiv a license to display the preprint in perpetuity. It is made available under aCC-BY-ND 4.0 International license.

anti-IL-6 treated mice (**Fig. 3 G**). Thus, cumulatively, our experiments showed that neither LC-derived nor total IL-6 plays a critical role in the induction of adaptive immune responses by steady-state LCs.

ICOS-ICOS-L signaling has no major role in the induction of adaptive immune responses by steady-state LCs

Since steady-state levels of IL-6 and type-I interferon had no significant role in inducing adaptive immune responses by LCs, we turned our attention to membrane-bound co-stimulation. ICOS-ICOS-L signaling, including on DCs, is required to induce Tfh cells and subsequent antibody responses in inflammatory settings (Choi et al., 2011; Weber et al., 2015; Pratama et al., 2015). To determine whether ICOS-ICOS-L interaction is involved in the induction of Tfh cells and antibody responses by steady-state LCs, we exposed Batf3$^{-/-}$ mice to ICOS-L blocking or isotype control antibodies (**Fig. 4 A, and S1 F**). The antigen-specific CD4^{+} T cell and B cell responses were characterized as discussed above. We found that blocking ICOS signaling minimally reduced the GC B cell but not antibody responses and did not affect the induction of GC-Tfh cells by steady-state LCs (**Fig. 4, B and C**). Thus, these data indicate that ICOS signaling is not critical in inducing adaptive immune responses by steady-state LCs.

CD80/CD86 on DCs are critical for the induction of adaptive immune responses by steady-state DCs

Since the inflammatory cytokines and co-stimulation previously identified as critical for Tfh differentiation and antibody responses had no significant role in inducing adaptive immune responses by steady-state LCs, we decided to establish an *in vitro* steady-state model to more efficiently test for DC-derived factors involved in the induction of the

bioRxiv preprint doi: https://doi.org/10.1101/2025.01.10.632426; this version posted January 14, 2025. The copyright holder for this preprint (which was not certified by peer review) is the author/funder, who has granted bioRxiv a license to display the preprint in perpetuity. It is made available under aCC-BY-ND 4.0 International license.

adaptive responses. For this *in vitro* platform, we used the MutuDC1 DC cells line (Fuertes Marraco et al., 2012), OT-II cells from a Rag2$^{-/-}$ background, and polyclonal primary B cells isolated from WT naïve mice (**Fig. 5 A**). The DCs and B cells were pulsed with OVA-peptide before co-culture, while cells not exposed to OVA served as controls. We anticipated that pulsing the polyclonal B cells with OVA-peptide should allow the cognate interaction with OT-II cells. Through this interaction, we expected that the B cells would provide the final maturation signals for the OT-II cells to differentiate into Tfh cells. In return, the T cells would facilitate the B cell responses, including isotype switching and antibody production. Indeed, we found that in the co-cultures where the DCs and the B cells were pulsed with OVA-peptide, the OT-II cells efficiently proliferated and differentiated into Tfh cells (**Fig. 5 B**). We also observed that a significant proportion of B cells underwent isotype switching and acquired GC phenotype (**Fig. 5 C**). We also detected substantial amounts of secreted IgG in the supernatant (data not shown). As expected, the inclusion of blocking MHC-II antibodies in the co-cultures prevented the T and B cell responses (**Fig. S2 A and B**). Furthermore, the primary DCs and MutuDC2 DC cell line (Pigni et al., 2018) in this co-culture assay also supported T and B cell responses but with different efficiencies (data not shown). Thus, we successfully established a steady-state co-culture system to study the induction of Tfh and B cell responses by DCs *in vitro*.

Having established the steady-state co-culture system, we next tested whether membrane-bound costimulatory molecules are involved in the T and B cell responses. We supplemented the co-cultures with blocking antibodies targeting CD40L (CD154), CD80/CD86, and ICOS-L (CD275) to test. We observed that blocking CD80 and CD86,

bioRxiv preprint doi: https://doi.org/10.1101/2025.01.10.632426; this version posted January 14, 2025. The copyright holder for this preprint (which was not certified by peer review) is the author/funder, who has granted bioRxiv a license to display the preprint in perpetuity. It is made available under aCC-BY-ND 4.0 International license.

but not the others, significantly inhibited the differentiation of Tfh cells and class-switched ($GL7^+IgD^-$) B cell responses (**Fig. 5, B and C, and Fig. S2 A and B**). Thus, CD80 and CD86 are critical in adaptive responses induced by steady-state DCs *in vitro*.

To confirm that CD80 and CD86 are also crucial in LC-induced responses *in vivo*, we repeated our LC-targeting experiments presented above in the presence of anti-CD80/CD86 or corresponding isotype antibodies (**Fig. 5 D**). We found that antibodies blocking CD80/CD86 signaling *in vivo* significantly inhibited the induction of Tfh cells by LCs (**Fig. 5 E**) and entirely suppressed B cell responses, including GC formation and antibody production (**Fig. 5 F**). Thus, membrane-bound co-stimulation through CD80/CD86 is critical for steady-state LC-induced adaptive immune responses.

In inflammatory settings, CD80/CD86 on DCs, but not on B cells, are required for adaptive T and B cell responses (Watanabe et al., 2017). To define whether those findings also apply to our steady-state antigen targeting model, we first used our *in vitro* co-culture assay presented above with slight modification. We co-cultured magnetically enriched migratory DCs from the SDLNs of WT or CD80/CD86 double knock-out (DKO) mice pulsed with anti-muLangerin-OVA or IgG4-OVA with OT-II T cells and WT or CD80/CD86 double knock-out B cells (**Fig. S2 C and D**). The Tfh cell differentiation was unaffected by the lack of CD80/CD86 on the B cells but was almost absent in cultures with DCs that lacked CD80/CD86 (**Fig. 5 G**). These data, therefore, support the idea that CD80/CD86 expression by DCs plays a critical role in the induction of Tfh cell responses.

In an attempt to confirm these *in vitro* findings *in vivo*, we generated bone marrow chimeras using the CD80/CD86 DKO, huLangerin, and $Batf3^{-/-}$ mice. We first irradiated

bioRxiv preprint doi: https://doi.org/10.1101/2025.01.10.632426; this version posted January 14, 2025. The copyright holder for this preprint (which was not certified by peer review) is the author/funder, who has granted bioRxiv a license to display the preprint in perpetuity. It is made available under aCC-BY-ND 4.0 International license.

CD80/CD86 DKO or huLangerin mice as previously described (Bouteau et al., 2019). The irradiated DKO mice were reconstituted with Batf3$^{-/-}$ bone marrow, while irradiated huLangerin mice were with DKO bone marrow. In the irradiated DKO chimeras reconstituted with Batf3$^{-/-}$ bone marrow, the LCs remain host origin and, as such, lack CD80/CD86. In the irradiated huLangerin mice reconstituted with DKO bone marrow, the only cell expressing CD80/CD86 would be the LCs expressing human Langerin targetable with the anti-huLangerin-Eα construct. We hypothesized that the resulting two chimeras would allow us to test whether LCs' CD80/CD86 is required and sufficient for the induction of Tfh cells and antibody responses. However, our analyses of bone marrow chimeras before use for interrogating T and B cell responses revealed that the DKO LCs became CD80/CD86 positive (**Fig. S2 E**) when reconstituted with Batf3$^{-/-}$ bone marrow, suggesting that LCs overcome their functional deficiency by picking up CD80/CD86 from the surrounding cells through intracellular monitoring (ICM), a phenomenon recently identified by our laboratory (Herbst et al., 2024). Thus, this prevented us from testing whether LC-restricted CD80/CD86 is required for adaptive immune responses. We also failed to test for sufficiency because irradiated huLangerin mice reconstituted with DKO bone marrow led to the elimination of the host huLangerin-expressing LCs (**Fig. S2 F**). Likely, CD80/CD86 reactive T cells from the DKO bone marrow mediated the rejection of host CD80/CD86 expressing LCs. Thus, because of these technical challenges, our *in vivo* efforts to confirm the *in vitro* findings have failed and remain to be further explored upon the discovery of ICM-specific blocking/interfering agents.

bioRxiv preprint doi: https://doi.org/10.1101/2025.01.10.632426; this version posted January 14, 2025. The copyright holder for this preprint (which was not certified by peer review) is the author/funder, who has granted bioRxiv a license to display the preprint in perpetuity. It is made available under aCC-BY-ND 4.0 International license.

In summary, we demonstrate that Langerhans cells (LCs) promote GC-Tfh and B cell responses in steady-state, independent of IL-6, type-I interferon, and ICOS signaling. However, we found that CD80/CD86 expression on DCs is essential for inducing these adaptive immune responses. These findings differentiate steady-state T cell differentiation from the conventional three-signal model of T cell differentiation in inflammatory settings, where cytokines are indispensable third signals.

The induction of humoral immune responses in the steady-state is not exclusive to LCs. Splenic cDC1s have also been reported to support Tfh and antibody responses, though their ability to do so, unlike LCs', depends on the receptor targeted (Steiner et al., 2022). In previous experiments, targeting migratory skin cDC1s through Langerin and Dectin-1 failed to elicit GC-Tfh or B cell responses, instead promoting cells with a pre-Tfh/Th1 phenotype (Bouteau et al., 2019). The reasons for these differences—whether due to distinct cDC1 subsets residing in different tissues (e.g., lymph nodes vs. spleen) or specific receptor targeting—remain to be elucidated. It will be crucial to investigate the instances when the cDC1s can support antibody responses, whether they undergo receptor-dependent alterations akin to those induced by inflammatory cues, such as IFN-α or poly-IC (Bouteau et al., 2019). As previously observed, cDC1-induced pre-Tfh/Th1 responses via Langerin targeting in steady-state were also independent of type-I interferons and IL-6 (Yao et al., 2015), further reinforcing that adaptive immune response induced by DCs in steady-state are independent of cytokines. Notably, in our model, no polarizing adjuvants or pattern recognition ligands were used that could directly or indirectly differentially affect LCs and cDC1s. Both subsets were targeted via the same receptor, yet they induced distinct adaptive immune responses. This strongly

bioRxiv preprint doi: https://doi.org/10.1101/2025.01.10.632426; this version posted January 14, 2025. The copyright holder for this preprint (which was not certified by peer review) is the author/funder, who has granted bioRxiv a license to display the preprint in perpetuity. It is made available under aCC-BY-ND 4.0 International license.

supports the idea that DC subsets are functionally specialized or pre-programmed, even in steady-state, to drive specific adaptive immune responses. Our findings align with studies on pre-committed DC precursors in the bone marrow (Satpathy et al., 2012; Schlitzer et al., 2015), suggesting that tissue residency might play a limited role in shaping the functional specialization of DC subsets. These results underscore the intrinsic programming of DC subsets in directing distinct immune pathways.

The findings that these prominent immunological factors in defining Tfh cell differentiation and B cell responses in our model do not seem to be critical contributors do not rule out that other cytokines or soluble factors might play a significant role in the process. However, our observations may offer insight into the mechanisms underlying homeostatic immunity toward commensals (Belkaid and Harrison, 2017) and the development of certain autoimmune diseases. Engagement of DCs by commensals through pattern recognition receptors, unlike pathogenic interactions, typically leads to no detectable or minimal activation and maturation (Ansaldo et al., 2021), suggesting limited involvement of DC-derived cytokines in polarizing commensal-specific T helper (Th) subsets. If cytokines are not critical in steady-state, what drives distinct Th responses? One possibility is that DC subsets differ in their peptide-MHC levels, a hypothesis aligned with the quantitative model proposed by van Panhuys and colleagues (Van Panhuys, 2016). However, our findings suggest that additional factors beyond peptide-MHC levels contribute to Tfh and B cell responses. LCs, across a wide range of antigen doses, while with different efficiency, uniquely support antibody responses (Yao et al., 2015; Bouteau et al., 2019), unlike cDC1s, which fail to do so under similar conditions. LCs appear to provide stronger cumulative TCR stimulation,

bioRxiv preprint doi: https://doi.org/10.1101/2025.01.10.632426; this version posted January 14, 2025. The copyright holder for this preprint (which was not certified by peer review) is the author/funder, who has granted bioRxiv a license to display the preprint in perpetuity. It is made available under aCC-BY-ND 4.0 International license.

evidenced by sustained CD69 expression, pS6 phosphorylation (Bouteau et al., 2019), and Nur77-GFP signals (unpublished observation) in T cells activated by LCs. Given that Tfh differentiation requires stronger TCR stimulation than Th1 differentiation (Bhattacharyya and Feng, 2020), this enhanced signal may explain the unique ability of LCs to promote Tfh cells. How LCs provide more potent stimuli than cDC1s and drive distinct adaptive immune responses in steady-state and inflammation (Igyártó et al., 2011) remains to be determined. While here we show that CD80/CD86 play an essential role in LC-induced adaptive immune responses, the contribution of CD80/CD86 as the second signal is likely not unique to LCs since other DCs in the lymph nodes also express high levels of CD80/CD86. Thus, other factors unique to these DC subsets, such as differentially expressed CD11a and CD11b integrins (Bouteau et al., 2019), molecules that play an essential role in regulating immunological synapses (Balkow et al., 2010; Varga et al., 2007), could likely serve as the decisive “third signal” and polarize the naïve T cells into distinct Th cells.

LCs and cDC1s exhibit distinct cytokine transcript profiles in the steady state, which may underlie their functional specialization (Igyártó et al., 2011). LCs are enriched in transcripts for *Il1b, Il6*, and *Il23p19*, aligning with their capacity to promote Th17 responses. Conversely, cDC1s harbor higher levels of *Il12p40* and *Il27* transcripts, correlating with their roles in driving Th1 and CTL responses. Interestingly, *Il12p40* transcript expression is detectable even in pre-committed bone marrow cDC1 precursors (Schlitzer et al., 2015), indicating intrinsic programming that primes DCs for rapid and specific cytokine production upon activation. These findings suggest that DC subsets are poised to respond swiftly to external stimuli by producing subset-specific

bioRxiv preprint doi: https://doi.org/10.1101/2025.01.10.632426; this version posted January 14, 2025. The copyright holder for this preprint (which was not certified by peer review) is the author/funder, who has granted bioRxiv a license to display the preprint in perpetuity. It is made available under aCC-BY-ND 4.0 International license.

cytokines that facilitate targeted Th polarization. However, our steady-state results indicate that cytokines may not be involved in the polarization of Th cells under non-inflammatory conditions. Therefore, we propose a model wherein, in the steady-state differential expression of adhesion molecules—such as integrins (CD11a and CD11b)—by DC subsets may provide a critical "third signal" to skew adaptive immune responses. These integrin-mediated could selectively promote “basic” Tfh, Th1, and potentially Th2 differentiation without the need for cytokine-mediated signaling. Under inflammatory conditions, cytokines would act as a "fourth signal," boosting and further polarizing the T helper cells into effector subsets, such us Th17, Th22, and others, tailored to combat the specific infection and restore tissue homeostasis. This dual-layered model highlights how DC subsets integrate their intrinsic programming with environmental cues to orchestrate adaptive immunity dynamically.

FIGURE LEGENDS

Figure 1. LCs, unlike cDC1s, induce GC-Tfh cells and antibody responses in steady-state. (**A**) LCs and cDC1s were quantified in the indicated mouse strains. Representative flow plots and summary graphs. Upstream gate: live/singlets, MHC-II^{hi}, CD11c^{+}, Langerin^{+}. Data was pooled from two independent experiments. Each dot represents a separate mouse. (**B**) The indicated mice were transferred with TEα cells and then immunized with 1 µg of anti-muLangerin-hIgG4-Eα or vehicle (PBS) the next day. Ag-specific TEα cell responses were assessed 4 days later by flow cytometry. Representative flow plots with corresponding summary graphs are shown. Upstream gate: live/singlets. TEα cells were identified as CD4^{+}CD90.1^{+}. For the subsequent plots, % of total TEα is shown. Data was pooled from two independent experiments. Each dot

bioRxiv preprint doi: https://doi.org/10.1101/2025.01.10.632426; this version posted January 14, 2025. The copyright holder for this preprint (which was not certified by peer review) is the author/funder, who has granted bioRxiv a license to display the preprint in perpetuity. It is made available under aCC-BY-ND 4.0 International license.

represents a separate mouse. (**C**) The mice were immunized with 1 µg of anti-huLangerin-hIgG4-Eα or vehicle (PBS), and fourteen days later, Ag-specific B cell responses were assessed by flow cytometry and (**D**) ELISA. Representative flow plots with corresponding summary graphs are shown. Upstream gate: live/singlets/dump. hIgG4-specific B cells were identified as $B220^{+}hIgG4^{+}$. For the subsequent plots, % of total hIgG4 is shown. Data was pooled from three independent experiments. Each dot represents a separate mouse. *p<0.05, **p<0.005, ns=not significant.

Figure 2. Type I interferon is not required for the induction of adaptive immune responses by steady-state LCs. (**A**) huLangCre-IFNαR1$^{f/f}$ mice were generated as depicted, which allowed us to target IFNαR1-deficient ($LC^{\Delta IFN\alpha R1}$) or -sufficient LCs. These mice were transferred with TEα cells and then immunized with 1 µg of anti-huLangerin-hIgG4-Eα the next day. Ag-specific TEα cell responses were assessed 4 days later by flow cytometry. At fourteen days, flow cytometry and ELISA, respectively, assessed Ag-specific T cell and B cell responses. (**B**) Representative contour plots of TEα cells with the percentage of Tfh cells ($PD1^{+}CXCR5^{+}$) and summary graphs, including Bcl-6 MFIs of the proliferated TEα cells. (**C**) Representative contour plots of Ag-specific B cells with percentage of GC B cells ($CD38^{-}GL7^{+}$) and summary graph. (**D**) hIgG4-specific mIgG serum levels defined by ELISA. Data from two independent experiments were pooled. Each dot represents a separate mouse. (**E**) The treatment plan of Batf3$^{-/-}$ mice with anti-IFNαR1 or isotype control antibody before and following LC targeting. (**F**) Left: the percentage of Tfh cells ($PD1^{+}CXCR5^{+}$) among proliferated TEα cells. Right: MFI of Bcl-6 of proliferated TEα cells. (**G**) Left: summary graph of Ag-specific GC B cells ($CD38^{-}GL7^{+}$), and right: hIgG4-specific mIgG serum levels defined

bioRxiv preprint doi: https://doi.org/10.1101/2025.01.10.632426; this version posted January 14, 2025. The copyright holder for this preprint (which was not certified by peer review) is the author/funder, who has granted bioRxiv a license to display the preprint in perpetuity. It is made available under aCC-BY-ND 4.0 International license.

by ELISA. Data from one representative experiment out of two is shown. Each dot represents a separate mouse. *p<0.05, ns=not significant.

Figure 3. IL-6 is not required for the induction of adaptive immune responses by steady-state LCs. (**A**) huLangCre-IL-6$^{f/f}$ mice were generated as depicted, which allowed targeting either IL-6-deficient (LC$^{\Delta IL\text{-}6}$) or IL-6-sufficient LCs. These mice were transferred with TEα cells and then immunized with 1 µg of anti-huLangerin-hIgG4-Eα the next day. Ag-specific TEα cell responses were assessed 4 days later by flow cytometry. At fourteen days, flow cytometry and ELISA assessed Ag-specific B cell responses. (**B**) Summary graphs on the percentage of Tfh cells (PD1$^+$CXCR5$^+$) and Bcl-6 MFIs of the proliferated TEα cells. (**C**) Summary graph on Ag-specific GC B cell percentages (CD38$^-$GL7$^+$), and hIgG4-specific mIgG serum levels defined by ELISA. Data from two independent experiments were pooled. Each dot represents a separate mouse. (**D**) The treatment plan of Batf3$^{-/-}$ mice with anti-IL-6 before and following LC targeting. (**E**) Left: the percentage of Tfh cells (PD1$^+$CXCR5$^+$) among proliferated TEα cells. Right: MFI of Bcl-6 of proliferated TEα cells. (**F**) Summary graph of Ag-specific GC B cells (CD38$^-$GL7$^+$) and (**G**) hIgG4-specific mIgG serum levels defined by ELISA. Data from one representative experiment out of two is shown. Each dot represents a separate mouse. *p<0.05, ns=not significant.

Figure 4. **ICOS-ICOS-L signaling has no major role in the induction of adaptive immune responses by steady-state LCs.** (**A**) The treatment plan of Batf3$^{-/-}$ mice with anti-ICOS-L before and following LC targeting to assess T- (left) and B cell responses (right). (**B**) Left: the percentage of Tfh cells (PD1$^+$CXCR5$^+$) among proliferated TEα cells. Right: MFI of Bcl-6 of proliferated TEα cells. Data from one representative

bioRxiv preprint doi: https://doi.org/10.1101/2025.01.10.632426; this version posted January 14, 2025. The copyright holder for this preprint (which was not certified by peer review) is the author/funder, who has granted bioRxiv a license to display the preprint in perpetuity. It is made available under aCC-BY-ND 4.0 International license.

experiment out of three is shown. (**C**) Left: summary graph of Ag-specific GC B cells ($CD38^{-}GL7^{+}$), and right: hIgG4-specific mIgG serum levels defined by ELISA. Data from two independent experiments were pooled. Each dot represents a separate mouse. *p<0.05, ns=not significant.

Figure 5. **CD80/CD86 on DCs are critical for the induction of adaptive immune responses by steady-state DCs.** (**A**) *In vitro* steady-state platform to model GC-dependent adaptive immune responses. (1) Murine DC cells (MutuDC1 cell line) and B cells enriched from WT mice were pulsed with OVA peptide. (2) Ag-specific $CD4^{+}$ T cells (OT-II) were added after washing off the peptide. (3) After 5 days, the phenotype of T and B cells was determined by flow cytometry. (**B**) The role of CD80/86 in adaptive immune responses was tested *in vitro*. Anti-CD80/86 blocking Ab (or an isotype control Ab) were added simultaneously with T cells. Five days later, the phenotype of T cells was assessed by flow cytometry. Representative dot plot of proliferated OT-II cells with percentage of Tfh cells ($PD1^{+}Bcl\text{-}6^{+}$). Summary graph: the number of Tfh cells in each well was calculated and plotted relative to the average of Tfh cells in isotype conditions. Data from two independent experiments were pooled. Each dot represents a separate replicate. (**C**) Representative dot plot of proliferated B cells with percentage of GC cells ($IgD^{-}GL7^{+}$). Summary graph: the number of GC B cells in each well was calculated and plotted relative to the average of GC B cells in isotype conditions. Data from two independent experiments were pooled. Each dot represents an independent replicate. (**D**) The treatment plan of $Batf3^{-/-}$ mice with anti-CD80/CD86 before and following LC targeting to assess T- (left) and B cell responses (right). (**E**) Representative TEα flow plots and summary graphs. Left: Total Tfh cells. Middle: The percentage of Tfh cells

bioRxiv preprint doi: https://doi.org/10.1101/2025.01.10.632426; this version posted January 14, 2025. The copyright holder for this preprint (which was not certified by peer review) is the author/funder, who has granted bioRxiv a license to display the preprint in perpetuity. It is made available under aCC-BY-ND 4.0 International license.

($PD1^+CXCR5^+$) among proliferated TEα cells. Right: MFI of Bcl-6 of proliferated TEα cells. Data from one representative experiment out of three is shown. Each dot represents a separate mouse. (**F**) Representative flow plots and summary graphs for antigen-specific B cells. Left: summary graph of Ag-specific GC B cells ($CD38^-GL7^+$), and right: hIgG4-specific mIgG serum levels defined by ELISA. Data from two independent experiments were pooled. Each dot represents a separate mouse. (**G**) To test the role of CD80/86 on DCs and B cells, DCs and B cells were isolated from WT of CD80/86 DKO mice. DCs and B cells were pulsed for 24h with OVA peptide attached to an anti-mLangerin Ab (or non-targeted Ab (hIgG)). Then, after washing, Ag-specific OT-II T cells were added. After 5 days, the phenotype of T cells was checked by flow cytometry. The number of Tfh cells in each well was calculated and plotted relative to the average Tfh cells in WT DC/WT B cell conditions. Data from two independent experiments were pooled. Each dot represents an independent replicate. *p<0.05, **p<0.005, ***p<0.001, ****p<0.0001, ns=not significant.

Figure S1. **Validation experiments for type I interferon, IL-6, and ICOS-L interference.** (**A**) huLangCre-IFNαR1$^{f/f}$ mice were generated to delete IFNαR1 in LCs specifically. SDLN of huLangCre-IFNαR1$^{f/f}$ mice (Cre+), littermate controls (Cre-) and IFNαR1 complete KO mice were stained for IFNαR1 by flow cytometry. MFI of IFNαR1 was calculated for B cells, cDC1s, LCs, and rDCs. Data from multiple experiments pooled together. Each dot represents a separate mouse. (**B**) Batf3$^{-/-}$ mice were treated with anti-IFNαR1 blocking Ab or an isotype. Four and fourteen days after LC targeting, SDLN were isolated and stained for IFNαR1 (same clone used *in vivo* to block the receptor). Left: representative histogram of B cells from isotype or anti-IFNαR1 treated

bioRxiv preprint doi: https://doi.org/10.1101/2025.01.10.632426; this version posted January 14, 2025. The copyright holder for this preprint (which was not certified by peer review) is the author/funder, who has granted bioRxiv a license to display the preprint in perpetuity. It is made available under aCC-BY-ND 4.0 International license.

mice. Shaded grey are B cells stained with an isotype control. Right: summary data of IFNαR1 staining on B cells. (**C**) LCs were targeted with 1 µg of anti-mLangerin-hIgG4 Ab in the absence or presence of IFNα. Fourteen days later, the percentage of GC-B cells among hIgG4 specific B cells was assessed by flow cytometry (left), and anti-hIgG4 Ab responses (right) were assessed by ELISA on serum. Data from two experiments pooled. Each dot represents a separate mouse. (**D**) huLangCRE-IL-6$^{f/f}$ mice were generated to target IL-6-deficient (LC$^{\Delta IL\text{-}6}$) or -sufficient LCs. LCs and keratinocytes (KC) of Cre+ and Cre- mice were sorted, and genomic DNA was extracted for genotyping. Note that the recombined band is only present in Cre+ LCs. (**E**) The serum of Batf3$^{-/-}$ mice treated with anti-IL-6 or isotype control antibodies was collected, and the concentration of IL-6 was assessed by Luminex. (**F**) The efficiency of ICOS-L blockade is shown. B cells were stained with anti-ICOS-L. Each dot represents a separate mouse. **p<0.005, ***p<0.001, ****p<0.0001, ns=not significant.

Figure S2. **Validation experiments for CD80/CD86 and other co-stimulatory molecules.** (**A**) The role of MHCII, CD154, CD275, CD80/86, or a combination of these parameters in GC responses was tested *in vitro*. Blocking Abs or isotype control Abs were added to the *in vitro* model simultaneously with T cells. Five days later, the phenotype of T cells (left) and B cells (right) was assessed by flow cytometry. The Tfh and GC B cells in each well were calculated and plotted relative to the average of Tfh and GC B cells in isotype conditions. Data from two independent experiments were pooled. Each dot represents an independent replicate. (**C**) At the end of the in vitro cultures with WT and CD80/86 DKO DCs and B cells, the level of CD86 on DCs and (**D**) B cells was determined by flow cytometry, and the MFI values of CD86 were plotted.

bioRxiv preprint doi: https://doi.org/10.1101/2025.01.10.632426; this version posted January 14, 2025. The copyright holder for this preprint (which was not certified by peer review) is the author/funder, who has granted bioRxiv a license to display the preprint in perpetuity. It is made available under aCC-BY-ND 4.0 International license.

Data from two independent experiments were pooled. (**E**) Bone marrow chimera model to test for the requirement of CD80/CD86 on LCs in driving the adaptive immune responses and the level of CD86 on LCs. (**F**). Bone marrow chimera model to test for the sufficiency of CD80/CD86 on LCs in driving the adaptive immune responses and the level of human Langerin on LCs.

MATERIALS AND METHODS

Mice

huLangerin (also called huLangerin-DTR) (Bobr et al., 2010), Batf3$^{-/-}$ (Edelson et al., 2010), and huLangerinCre (Kaplan et al., 2007) mice have been previously described. huLangerinCre were crossed with IFNαR1$^{f/f}$ (Jackson Laboratories strain 028256) or IL-6$^{f/f}$ (mice provided by Dr. Roger Davis, University of Massachusetts; developed by Dr. Juan Hidalgo at Universitat Autònoma de Barcelona) (Sanchis et al., 2020). CD90.1 congenic TEα Rag1$^{-/-}$ CD4 TCR transgenic mice to I-Eα_{52-68} on the C57BL/6 background were initially obtained from Dr. Marc Jenkins (University of Minnesota). IRF8$^{32\Delta}$ mice were obtained from Dr. Kenneth Murphy (Washington University School of Medicine) and Jackson Laboratories. XCR1-Cre-DTA mice were generated by crossing XCR1-Cre (Jackson Laboratories strain 035435; developed by Dr. Kenneth Murphy) with “STOP”-DTA (Jackson Laboratories strain 009669). WT C57BL/6J (strain 000664), CD45.1 PepBoy (strain 002014), and OT-II (strain 005194) were purchased from Jackson Laboratories and maintained in our facility. Rag2$^{-/-}$ OT-II mice were purchased from Taconic model 11490. CD80/86 double knock-out (DKO) mice developed by Dr. Arlene H. Sharpe (Mass General Hospital and Harvard Medical School) (Borriello et al., 1997) was provided by Drs. Masashi Watanabe and Richard Hodes (NIH). All

bioRxiv preprint doi: https://doi.org/10.1101/2025.01.10.632426; this version posted January 14, 2025. The copyright holder for this preprint (which was not certified by peer review) is the author/funder, who has granted bioRxiv a license to display the preprint in perpetuity. It is made available under aCC-BY-ND 4.0 International license.

experiments were performed with 6- to 12-week-old female and male mice. Mice were housed in microisolator cages and fed autoclaved food and water. The Institutional Care and Use Committee at Thomas Jefferson University approved all mouse protocols under protocol number: 02315.

Steady-state Langerin targeting

These experiments were performed with anti-human/anti-mouse mAb and conjugates (anti-huLangerin-Eα, anti-muLangerin-Eα anti-muLangerin-doc, cohesin-IFNα4) generated in-house, as previously described (Bouteau et al., 2019). All the reagents used in this study were generated using mammalian cell lines to minimize the presence of endotoxins. The average endotoxin level was below 0.2 ng LPS/mg protein. Eα (I-Eα_{52-68}) is a well-characterized immunodominant T cell epitope from the I-Eα MHCII molecule recognized by transgenic TEα cells in the context of I-A_β. For the generation of the anti-muLangerin-IFNα4 construct, we used a previously described technology that relies on the high-affinity interactions between dockerin (doc) and cohesin (coh) (Bouteau et al., 2019). Dockerin was fused to the heavy chain of the antibody. Mice received intravenous (i.v.) transfer of CFSE-labeled, congenically marked $3x10^5$ TEα cells 1 day before antigen targeting as previously described (Bouteau et al., 2019). One µg of anti-human/anti-mouse mAb and conjugates or PBS were administered intraperitoneally (i.p.) on day 0. For TEα cells characterization, mice were sacrificed 4 days after Langerin targeting, and the skin-draining lymph nodes (SDLNs; axillary, brachial, and inguinal) were harvested for flow cytometry. For B cell characterization, mice were sacrificed on day fourteen, the SDLNs were harvested for flow cytometry, and the blood was collected for serum isolation and ELISA. For dendritic cell

bioRxiv preprint doi: https://doi.org/10.1101/2025.01.10.632426; this version posted January 14, 2025. The copyright holder for this preprint (which was not certified by peer review) is the author/funder, who has granted bioRxiv a license to display the preprint in perpetuity. It is made available under aCC-BY-ND 4.0 International license.

characterization, SDLNs were digested as described previously (Bouteau et al., 2019) before staining for flow cytometry.

Flow cytometry

Flow cytometry was performed on single-cell suspensions of the SDLNs (axillary, brachial, and inguinal) of mice. The fixable viability dye (Thermo Fisher Scientific) was used to exclude dead cells. The following antibodies from BioLegend were used to stain cells CD3 (145-2C11), CD4 (GK1.5), CD16/CD32 (93), CD19 (6D5), CD25 (PC61), CD44 (IM7), CD45.2 (104), CD69 (H1.2F3), CD80 (16-10A1), CD86 (GL-1), CD90.2 (30-H12), CD138 (281-2), CD275 (HK5.3), B220 (RA3-6B2), Blimp1 (5E7), CXCR5 (L138D7), GL7 (GL7), IFNaR1 (MAR1-5A3), IgD (11-26c.2a), IgM (RMM-1), MHCII (M5/114.15.2), PD-1 (29F.1A12),and Sca1 (D7). CD4 (GK1.5), CD38 (90), CD90.1 (OX-7), Bcl6 (K112-91), and IgD (D7) were purchased from BD Biosciences. CD11b (M1/70), CD90.2 (53-2.1), F4/80 (BM8) were purchased from Thermo Fisher Scientific. For antigen-specific B cell staining, cells were also incubated *ex vivo* with AF647-conjugated targeting Ab construct. Intracellular transcription factor staining was performed with the BD Bioscience Cytofix/Cytoperm kit (BD Biosciences, San Jose, CA), according to the manufacturer's instructions. All the flow cytometric plots presented in this article were pre-gated on live (using Live/Dead stain) and singlet events. Samples were analyzed on an LSRFortessa or Symphony flow cytometer (BD Biosciences), and data were analyzed with FlowJo software (BD Biosciences).

Assessment of Humoral Immune Responses by ELISA

Serum samples were obtained 14 days after immunization with anti-Langerin Ab constructs using BD Microtainer SST tubes (BD) and stored at −80°C. To determine

bioRxiv preprint doi: https://doi.org/10.1101/2025.01.10.632426; this version posted January 14, 2025. The copyright holder for this preprint (which was not certified by peer review) is the author/funder, who has granted bioRxiv a license to display the preprint in perpetuity. It is made available under aCC-BY-ND 4.0 International license.

antigen-specific antibody titers, clear flat-bottom immune 96-well plates were coated with 50 µL of huIgG4 protein diluted in BupH Carbonate-Bicarbonate buffer (Thermo Fisher Scientific) at 2 µg of protein/ml and incubated overnight at 37C. After washing, plates were blocked with blocking buffer (TBS; Thermo Fisher Scientific). After blocking, the buffer was discarded, and serial dilutions of serum in the blocking buffer were added and incubated for 2 h at 37°C. A serial dilution of a mouse anti-hIgG4 antibody (EMD Millipore) was used as a standard. After washing, plates were incubated with horseradish peroxidase (HRP)–conjugated goat anti-mouse IgG (Jackson ImmunoResearch; West Grove, PA) in blocking solution for 2 h at 37°C, washed and developed with HRP substrate (Ultra-TMB Chromogen Solution: ThermoFisher Scientific). The reaction was stopped with 1N HCl and plates were read at 450 nm.

IFNαR1 antibody *in vivo* treatment

For blockade of IFNαR1, Batf3$^{-/-}$ mice were treated with 0.5 mg/mouse of IFNαR1 blocking antibody (clone MAR1-5A3; BioLegend) on 3 consecutive days pre-immunization and 0.25 mg every 3 days post-immunization (Macal et al., 2018). Control mice received a similar amount of a mouse IgG1 isotype control antibody (clone MOPC-21; BioLegend). All antibodies were administrated i.v. in 300 µl of PBS. To validate the block, SDLNs were isolated and stained for IFNαR1 (the same clone used *in vivo* to block the receptor).

IL-6 antibody *in vivo* treatment

For the blockade of IL-6, Batf3$^{-/-}$ mice were treated with 0.5 mg/mouse of IL-6 blocking antibody (clone MP5-20F3; BioLegend) on one-day pre-immunization and 0.25 mg every other day post-immunization. Control mice received a similar amount of a rat IgG1

bioRxiv preprint doi: https://doi.org/10.1101/2025.01.10.632426; this version posted January 14, 2025. The copyright holder for this preprint (which was not certified by peer review) is the author/funder, who has granted bioRxiv a license to display the preprint in perpetuity. It is made available under aCC-BY-ND 4.0 International license.

isotype control antibody (clone RTK2071; BioLegend). All antibodies were administrated i.v. in 300 µl of PBS. To validate the block, the blood of each mouse was collected, and serum was isolated for Luminex® analysis.

ICOS-L antibody *in vivo* treatment

For blockade of ICOS-L (CD275) and TEα cell characterization, Batf3$^{-/-}$ mice were treated with 0.1 mg/mouse of ICOS-L blocking antibody (clone HK5.3; BioLegend) on days -8, -7, and -6 pre-immunization. CFSE-labeled TEα cells were transferred on day -1. Control mice received a similar amount of a rat IgG2a isotype control antibody (clone RTK2758; BioLegend). All antibodies were administrated i.v. in 300 µl of PBS. For blockade of ICOS-L (CD275) and B cell characterization, Batf3$^{-/-}$ mice were treated with 0.1 mg/mouse of ICOSL blocking antibody (clone HK5.3; BioLegend) on day -1 pre-immunization, and days 1 and 7 post-immunization. Control mice received a similar amount of a rat IgG2a isotype control antibody (clone RTK2758; Biolegend). All antibodies were administrated i.v. in 300 µl of PBS. To validate the block, the blood of each mouse was collected and stained for ICOS-L with the exact clone as the antibody used for the *in vivo* treatment.

CD80/86 antibodies *in vivo* treatment

For blockade of CD80 and CD86 and TEα cell characterization, Batf3$^{-/-}$ mice were treated with 0.15 mg/mouse of CD80 (clone 16-10A1; BioXCell) and 0.15 mg/mouse of CD86 (clone GL-1; BioXCell) blocking antibodies on days -1, 0, and 1 (relative to immunization day). Control mice received a similar amount of a rat IgG2a isotype control antibody (clone RTK2758; BioLegend). All antibodies were administrated i.p. in 100 µl of PBS. For blockade of CD80 and CD86 and B cell characterization, Batf3$^{-/-}$

bioRxiv preprint doi: https://doi.org/10.1101/2025.01.10.632426; this version posted January 14, 2025. The copyright holder for this preprint (which was not certified by peer review) is the author/funder, who has granted bioRxiv a license to display the preprint in perpetuity. It is made available under aCC-BY-ND 4.0 International license.

mice were treated with 0.15 mg/mouse of CD80 (clone 16-10A1; BioXCell) and 0.15 mg/mouse of CD86 (clone GL-1; BioXCell) blocking antibodies on days 0, 1, 2 and 3. Control mice received rat IgG2a and Armenian hamster IgG isotype control antibodies (clones 2A3 and BE0091, respectively; BioXCell). All antibodies were administrated i.p. in 100 µl of PBS. SDLNs were stained with CD80 and CD86 antibodies to validate the block (same clone as the antibodies used for the *in vivo* treatment).

***In vitro* assay with MutuDC1**

For this assay, we combined and optimized protocols from P. Sage and A. Sharpe (Sage and Sharpe, 2015) and Kolenbrander et al., (Kolenbrander et al., 2018).

Cells were prepared in co-culture in 96-well U-bottom plate as follows: 1) (**ref**) 10^4 MutuDC1 cells/well were distributed in complete IMDM (IMDM w/ Glutamax w/ HEPES, 8% Heat-inactivated FBS, 50 µM β-mercaptoethanol and 1% pen/strep). 2) B cells were labeled with Cell-Trace Yellow (BioLegend) and enriched (Mojosort pan-B cell selection kit from BioLegend) from the spleen of CD45.1 mice. $2.5x10^5$ CD45.1 B cells were distributed in the same wells as MutuDC1. 3) MutuDC1 and B cells were pulsed at 15 µg/mL with $OVA_{323-339}$ peptide (GenScript) for 1 hour at 37°C 5% CO_2. 4) Rag2/OT-II T cells were isolated from spleen, mesenteric and SDLNs and labeled with Cell-Trace Violet (BioLegend). After washing MutuDC1 and B cells with complete IMDM twice, $5x10^5$ Rag2/OT-II T cells were added per well. 5) After mixing, cells were incubated for 5 days at 37°C 5% CO_2.

Different controls lacking different cell populations or peptides were used. If any blocking antibodies were added to wells, it was at the same time as the addition of T cells at 5 µg/mL. Blocking antibodies used were MHC-II block (clone Y-3P from

bioRxiv preprint doi: https://doi.org/10.1101/2025.01.10.632426; this version posted January 14, 2025. The copyright holder for this preprint (which was not certified by peer review) is the author/funder, who has granted bioRxiv a license to display the preprint in perpetuity. It is made available under aCC-BY-ND 4.0 International license.

BioXCell), CD80 (clone 16-10A1 from BioLegend); CD86 (clone GL-1 from BioLegend); CD154 (clone MR1 from BioLegend); CD275 (clone HK5.3 from BioLegend). At the end of the incubation, the plate was centrifuged. The supernatant was used for ELISA mIg detection. Briefly, clear flat-bottom immune 96-well plates were coated with 50 µL of F(ab')2 Donkey anti-mouse IgG (H+L) (ThermoFisher Scientific) diluted at 8 µg/mL in BupH Carbonate-Bicarbonate buffer (Thermo Fisher Scientific) and incubated overnight at 37°C. After washing with PBS + Tween20 (ThermoFisher Scientific), plates were blocked with a 2% milk solution for 30 minutes at 37°C. After washing, serial dilutions of supernatant in TBS were added and incubated for 2 h at 37°C. After washing, plates were incubated with horseradish peroxidase (HRP)–conjugated Donkey anti-mouse IgG (H+L) (ThermoFisher Scientific) in TBS for 2 h at 37°C, washed and developed with HRP substrate (Ultra-TMB Chromogen Solution: ThermoFisher Scientific). The reaction was stopped with 1N HCl and plates were read at 450 nm.

The cells were stained with the following antibodies: CD4 (GK1.5; BD Biosciences), CD44 (IM7; BioLegend), CD45.1 (A20; BioLegend), PD1 (39F.1A12; BioLegend), Bcl6 (K112-91; BD Biosciences), GL7 (GL7; BioLegend), IgD (11-26c.2a; BioLegend), CD19 (6D5; BioLegend), CD16/30 (93; BioLegend), and a fixable live/dead from Thermofischer Scientific.

***In vitro* assay with primary DCs**

This assay is similar to the *in vitro* assay with MutuDC1 with the following differences. The primary DC fraction was a CD11c positive enrichment (Mouse CD11c positive selection kit II from StemCell) of SDLNs of WT and CD80/86 DKO mice. The T cell fraction is a CD4 T cell enrichment (Mojosort mouse CD4 T cell enrichment from

bioRxiv preprint doi: https://doi.org/10.1101/2025.01.10.632426; this version posted January 14, 2025. The copyright holder for this preprint (which was not certified by peer review) is the author/funder, who has granted bioRxiv a license to display the preprint in perpetuity. It is made available under aCC-BY-ND 4.0 International license.

BioLegend) of spleen mesenteric and SDLN of OT-II mice. The B cell fraction is a B cell enrichment (Mouse Pan-B cell enrichment from BioLegend) of WT and CD80/86 DKO mice spleens. The antigen used here is anti-muLangerin-doc/cohesin-OTII (and control IgG4-doc/cohesion-OTII) generated in-house, as previously described (Bouteau et al., 2019). Primary DC ($5x10^4$ cells) and B cell (10^6 cells) fractions were pulsed for 24 hours at 37°C 5% CO_2 with 10nM of the targeting or control constructs. After washing, 10^5 cells of the T cell fraction were added and incubated for 5 more days at 37°C 5% CO_2. The staining of the cells at the end of the co-culture assay included the following antibodies from BD Biosciences: CD4 (GK1.5), CD38 (90) and Bcl-6 (K112-91). ThermoFisher Scientific antibodies used were specific for MHCII (M5/114.15.2), CD4 (GK1.5), CD86 (GL1), and the fixable live/dead marker. The following antibodies were purchased from BioLegend: CD44 (IM7), CD45.1 (A20), CD138 (281-2), IgD (11-26c.2a), CD19 (6D5), GL7 (GL7), CD11c (N418), PD1 (29F.1A12), and CD16/32 (93).

Generation of Bone Marrow Chimeras

Bone marrow cells were harvested from the tibia and femur of $Batf3^{-/-}$ or CD80/86 DKO donor mice as previously described (Bouteau et al., 2019). The recipient mice were irradiated (900cGy X-ray in X-rad 320 irradiator) and reconstituted with 10–20 million bone marrow cells/mouse via the tail vein as follows: 1) recipient-irradiated DKO (or control WT) mice were reconstituted with $Batf3^{-/-}$ bone marrow, and 2) irradiated huLangerin mice were reconstituted with DKO (or control WT) bone marrow. Eight weeks after bone marrow transfer, Langerhans cells from SDLNs were stained to determine the level of expression of CD86 or human Langerin with the following antibodies: CD11b (M1/70; BD Biosciences), CD19 (6D5; BioLegend), CD80 (16-10A1;

bioRxiv preprint doi: https://doi.org/10.1101/2025.01.10.632426; this version posted January 14, 2025. The copyright holder for this preprint (which was not certified by peer review) is the author/funder, who has granted bioRxiv a license to display the preprint in perpetuity. It is made available under aCC-BY-ND 4.0 International license.

BioLegend), CD11c (N418; BioLegend), CD207 (929F3.01 recognizing both mouse and human langerin; Novus Biologicals), CD103 (2E7; BioLegend), CD86 (GL-1; BioLegend), CD207 (2G3 recognizes only human langerin; in house) and MHCII (M5/114.15.2; BioLegend).

Statistical Analysis

Differences between 2 data sets were analyzed first for normality using the Shapiro-Wilk test. If normality was met, an unpaired t-test was used to assess the difference between the 2 different data sets. In the absence of normality, a Mann-Whitney test was used. For data sets with more than two groups, an ordinary one-way ANOVA with multiple comparisons was used. All analysis were performed with GraphPad Prism software.

ACKNOWLEDGMENTS

We thank the BioImaging Shared Resources, Flow Cytometry, and Laboratory Animal Facilities at Sidney Kimmel Cancer Center for their expert assistance in performing the presented experiments. We thank Dr. Hans Acha-Orbea for sharing the MutuDC cell lines. We thank Dr. Luis Sigal for sharing the IFNαR^{KO} mice, Drs. Arlene Sharpe, Masashi Watanabe, and Richard Hodes for the CD80/CD86^{DKO} mice, Drs. Juan Hidalgo and Roger Davis for the IL-6 floxed mice, and Dr. Kenneth Murphy for the IRF8$^{32\Delta}$ mice. Jerome Ellis and Zhiqing Wang are thanked for reagent making, and Jiukai Yu for laboratory assistance. Some of the figures were generated using BioRender. This work was supported by the National Institute of Allergy and Infectious Diseases (https://www.niaid.nih.gov) R01AI146420 to B.Z.I. and institutional start-up funds. The Flow Cytometry and Laboratory Animal Facilities at Sidney Kimmel Cancer Center at

bioRxiv preprint doi: https://doi.org/10.1101/2025.01.10.632426; this version posted January 14, 2025. The copyright holder for this preprint (which was not certified by peer review) is the author/funder, who has granted bioRxiv a license to display the preprint in perpetuity. It is made available under aCC-BY-ND 4.0 International license.

Thomas Jefferson University are supported by the National Cancer Institute (https://www.cancer.gov) P30CA056036.

AUTHORS CONTRIBUTIONS

A.B., Z.Q., and B.Z.I. designed experiments. A.B. and Z.Q. performed experiments, analyzed the data, and generated the figures. S.Z. and G.Z. supervised in-house reagent making and quality assurance and performed Luminex assays. B.Z.I. wrote the manuscript. All authors participated in discussions of experimental results, edited the manuscript, and approved the final manuscript.

DECLARATION OF INTERESTS

G.Z. and S.Z. are named inventors on BS&W Research Institute patent applications directed to the use of Langerin targeting. Other authors declare no competing interests.

REFERENCES

Ansaldo, E., T.K. Farley, and Y. Belkaid. 2021. Control of Immunity by the Microbiota. *Annu Rev Immunol*. 39:449–479. doi:10.1146/annurev-immunol-093019-112348.

Balkow, S., S. Heinz, P. Schmidbauer, W. Kolanus, B. Holzmann, S. Grabbe, and M. Laschinger. 2010. LFA-1 activity state on dendritic cells regulates contact duration with T cells and promotes T-cell priming. *Blood*. 116:1885–1894. doi:10.1182/blood-2009-05-224428.

Belkaid, Y., and O.J. Harrison. 2017. Homeostatic Immunity and the Microbiota. *Immunity*. 46:562–576. doi:10.1016/j.immuni.2017.04.008.

Bhattacharyya, N.D., and C.G. Feng. 2020. Regulation of T Helper Cell Fate by TCR Signal Strength. *Front Immunol*. 11. doi:10.3389/fimmu.2020.00624.

Bobr, A., I. Olvera-Gomez, B.Z. Igyártó, K.M. Haley, K.A. Hogquist, and D.H. Kaplan. 2010. Acute ablation of Langerhans cells enhances skin immune responses. *J Immunol*. 185:4724–4728.

Borriello, F., M.P. Sethna, S.D. Boyd, A.N. Schweitzer, E.A. Tivol, D. Jacoby, T.B. Strom, E.M. Simpson, G.J. Freeman, and A.H. Sharpe. 1997. B7-1 and B7-2 Have Overlapping, Critical Roles in Immunoglobulin Class Switching and Germinal Center Formation. *Immunity*. 6:303–313. doi:10.1016/S1074-7613(00)80333-7.

Bouteau, A., J. Kervevan, Q. Su, S.M. Zurawski, V. Contreras, N. Dereuddre-Bosquet, R. Le Grand, G. Zurawski, S. Cardinaud, Y. Levy, and B.Z. Igyártó. 2019. DC

bioRxiv preprint doi: https://doi.org/10.1101/2025.01.10.632426; this version posted January 14, 2025. The copyright holder for this preprint (which was not certified by peer review) is the author/funder, who has granted bioRxiv a license to display the preprint in perpetuity. It is made available under aCC-BY-ND 4.0 International license.

Subsets Regulate Humoral Immune Responses by Supporting the Differentiation of Distinct Tfh Cells. *Front Immunol*. 10. doi:10.3389/fimmu.2019.01134.

Caminschi, I., A.I. Proietto, F. Ahmet, S. Kitsoulis, J.S. Teh, J.C.Y. Lo, A. Rizzitelli, L. Wu, D. Vremec, S.L.H. Van Dommelen, I.K. Campbell, E. Maraskovsky, H. Braley, G.M. Davey, P. Mottram, N. Van De Velde, K. Jensen, A.M. Lew, M.D. Wright, W.R. Heath, K. Shortman, and M.H. Lahoud. 2008. The dendritic cell subtype-restricted C-type lectin Clec9A is a target for vaccine enhancement. *Blood*. 112:3264–3273. doi:10.1182/blood-2008-05-155176.

Caminschi, I., and K. Shortman. 2012. Boosting antibody responses by targeting antigens to dendritic cells. *Trends Immunol*. 33:71–77.

Carotta, S., S.N. Willis, J. Hasbold, M. Inouye, S.H.M. Pang, D. Emslie, A. Light, M. Chopin, W. Shi, H. Wang, H.C. Morse, D.M. Tarlinton, L.M. Corcoran, P.D. Hodgkin, and S.L. Nutt. 2014. The transcription factors IRF8 and PU.1 negatively regulate plasma cell differentiation. *Journal of Experimental Medicine*. 211:2169–2181. doi:10.1084/jem.20140425.

Choi, Y.S., R. Kageyama, D. Eto, T.C. Escobar, R.J. Johnston, L. Monticelli, C. Lao, and S. Crotty. 2011. ICOS receptor instructs T follicular helper cell versus effector cell differentiation via induction of the transcriptional repressor Bcl6. *Immunity*. 34:932–946.

Corbett, A.J., I. Caminschi, B.S. McKenzie, J.L. Brady, M.D. Wright, P.L. Mottram, P.M. Hogarth, A.N. Hodder, Y. Zhan, D.M. Tarlinton, K. Shortman, and A.M. Lew. 2005. Antigen delivery via two molecules on the CD8- dendritic cell subset induces humoral immunity in the absence of conventional “danger”. *Eur J Immunol*. 35:2815–2825.

Crotty, S. 2014. T follicular helper cell differentiation, function, and roles in disease. *Immunity*. 41:529–542.

Crotty, S. 2019. T Follicular Helper Cell Biology: A Decade of Discovery and Diseases. *Immunity*. 50:1132–1148. doi:10.1016/j.immuni.2019.04.011.

Cucak, H., U. Yrlid, B. Reizis, U. Kalinke, and B. Johansson-Lindbom. 2009. Type I interferon signaling in dendritic cells stimulates the development of lymph-node-resident T follicular helper cells. *Immunity*. 31:491–501.

Curtsinger, J.M., C.S. Schmidt, A. Mondino, D.C. Lins, R.M. Kedl, M.K. Jenkins, and M.F. Mescher. 1999. Inflammatory Cytokines Provide a Third Signal for Activation of Naive CD4+ and CD8+ T Cells1. *The Journal of Immunology*. 162:3256–3262. doi:10.4049/jimmunol.162.6.3256.

Doebel, T., B. Voisin, and K. Nagao. 2017. Langerhans Cells - The Macrophage in Dendritic Cell Clothing. *Trends Immunol*. 38:817–828. doi:10.1016/J.IT.2017.06.008.

Durai, V., P. Bagadia, J.M. Granja, A.T. Satpathy, D.H. Kulkarni, J.T. Davidson, R. Wu, S.J. Patel, A. Iwata, T.T. Liu, X. Huang, C.G. Briseño, G.E. Grajales-Reyes, M. Wöhner, H. Tagoh, B.L. Kee, R.D. Newberry, M. Busslinger, H.Y. Chang, T.L. Murphy, and K.M. Murphy. 2019. Cryptic activation of an Irf8 enhancer governs cDC1 fate specification. *Nat Immunol*. 20:1161–1173. doi:10.1038/s41590-019-0450-x.

Edelson, B.T., W. KC, R. Juang, M. Kohyama, L.A. Benoit, P.A. Klekotka, C. Moon, J.C. Albring, W. Ise, D.G. Michael, D. Bhattacharya, T.S. Stappenbeck, M.J. Holtzman,

bioRxiv preprint doi: https://doi.org/10.1101/2025.01.10.632426; this version posted January 14, 2025. The copyright holder for this preprint (which was not certified by peer review) is the author/funder, who has granted bioRxiv a license to display the preprint in perpetuity. It is made available under aCC-BY-ND 4.0 International license.

S.-S.J. Sung, T.L. Murphy, K. Hildner, and K.M. Murphy. 2010. Peripheral CD103+ dendritic cells form a unified subset developmentally related to CD8alpha+ conventional dendritic cells. *J Exp Med*. 207:823–836.

Ferris, S.T., V. Durai, R. Wu, D.J. Theisen, J.P. Ward, M.D. Bern, J.T. Davidson, P. Bagadia, T. Liu, C.G. Briseño, L. Li, W.E. Gillanders, G.F. Wu, W.M. Yokoyama, T.L. Murphy, R.D. Schreiber, and K.M. Murphy. 2020. cDC1 prime and are licensed by CD4+ T cells to induce anti-tumour immunity. *Nature*. 584:624–629. doi:10.1038/s41586-020-2611-3.

Fuertes Marraco, S.A., F. Grosjean, A. Duval, M. Rosa, C. Lavanchy, D. Ashok, S. Haller, L.A. Otten, Q.-G. Steiner, P. Descombes, C.A. Luber, F. Meissner, M. Mann, L. Szeles, W. Reith, and H. Acha-Orbea. 2012. Novel Murine Dendritic Cell Lines: A Powerful Auxiliary Tool for Dendritic Cell Research. *Front Immunol*. 3. doi:10.3389/fimmu.2012.00331.

Ginhoux, F., F. Tacke, V. Angeli, M. Bogunovic, M. Loubeau, X.-M. Dai, E.R. Stanley, G.J. Randolph, and M. Merad. 2006. Langerhans cells arise from monocytes in vivo. *Nat Immunol*. 7:265–273.

Herbst, C.H., A. Bouteau, E.J. Menykő, Z. Qin, E. Gyenge, Q. Su, V. Cooper, N.A. Mabbott, and B.Z. Igyártó. 2024. Dendritic cells overcome Cre/Lox induced gene deficiency by siphoning cytosolic material from surrounding cells. *iScience*. 27. doi:10.1016/j.isci.2024.109119.

Hilligan, K.L., and F. Ronchese. 2020. Antigen presentation by dendritic cells and their instruction of CD4+ T helper cell responses. *Cell Mol Immunol*. 17:587–599. doi:10.1038/s41423-020-0465-0.

Hoeffel, G., Y. Wang, M. Greter, P. See, P. Teo, B. Malleret, M. Leboeuf, D. Low, G. Oller, F. Almeida, S.H.Y. Choy, M. Grisotto, L. Renia, S.J. Conway, E.R. Stanley, J.K.Y. Chan, L.G. Ng, I.M. Samokhvalov, M. Merad, and F. Ginhoux. 2012. Adult Langerhans cells derive predominantly from embryonic fetal liver monocytes with a minor contribution of yolk sac-derived macrophages. *Journal of Experimental Medicine*. doi:10.1084/jem.20120340.

Igyártó, B.Z., K. Haley, D. Ortner, A. Bobr, M. Gerami-Nejad, B.T. Edelson, S.M. Zurawski, B. Malissen, G. Zurawski, J. Berman, and D.H. Kaplan. 2011. Skin-resident murine dendritic cell subsets promote distinct and opposing antigen-specific T helper cell responses. *Immunity*. 35:260–272.

Janeway, C.A., and R. Medzhitov. 2002. Innate immune recognition. *Annu Rev Immunol*. 20:197–216. doi:10.1146/annurev.immunol.20.083001.084359.

Kaplan, D.H. 2017. Ontogeny and function of murine epidermal Langerhans cells. *Nat Immunol*. 18:1068–1075.

Kaplan, D.H., M.C. Jenison, S. Saeland, W.D. Shlomchik, and M.J. Shlomchik. 2005. Epidermal langerhans cell-deficient mice develop enhanced contact hypersensitivity. *Immunity*. 23:611–620.

Kaplan, D.H., M.O. Li, M.C. Jenison, W.D. Shlomchik, R.A. Flavell, and M.J. Shlomchik. 2007. Autocrine/paracrine TGFbeta1 is required for the development of epidermal Langerhans cells. *J Exp Med*. 204:2545–2552.

Kato, Y., T.M. Steiner, H.-Y. Park, R.O. Hitchcock, A. Zaid, J.L. Hor, S. Devi, G.M. Davey, D. Vremec, K.M. Tullett, P.S. Tan, F. Ahmet, S.N. Mueller, S. Alonso, D.M. Tarlinton, H.L. Ploegh, T. Kaisho, L. Beattie, J.H. Manton, D. Fernandez-Ruiz, K.

bioRxiv preprint doi: https://doi.org/10.1101/2025.01.10.632426; this version posted January 14, 2025. The copyright holder for this preprint (which was not certified by peer review) is the author/funder, who has granted bioRxiv a license to display the preprint in perpetuity. It is made available under aCC-BY-ND 4.0 International license.

Shortman, M.H. Lahoud, W.R. Heath, and I. Caminschi. 2020. Display of Native Antigen on cDC1 That Have Spatial Access to Both T and B Cells Underlies Efficient Humoral Vaccination. *The Journal of Immunology*. 205:1842–1856. doi:10.4049/jimmunol.2000549.

Kato, Y., A. Zaid, G.M. Davey, S.N. Mueller, S.L. Nutt, D. Zotos, D.M. Tarlinton, K. Shortman, M.H. Lahoud, W.R. Heath, and I. Caminschi. 2015. Targeting Antigen to Clec9A Primes Follicular Th Cell Memory Responses Capable of Robust Recall. *J Immunol*. 195:1006–1014.

Kolenbrander, A., B. Grewe, D. Nemazee, K. Überla, and V. Temchura. 2018. Generation of T follicular helper cells in vitro: requirement for B-cell receptor cross-linking and cognate B- and T-cell interaction. *Immunology*. 153:214–224. doi:10.1111/imm.12834.

Krishnaswamy, J.K., S. Alsén, U. Yrlid, S.C. Eisenbarth, and A. Williams. 2018. Determination of T Follicular Helper Cell Fate by Dendritic Cells. *Front Immunol*. 9. doi:10.3389/fimmu.2018.02169.

Lahoud, M.H., F. Ahmet, S. Kitsoulis, S.S. Wan, D. Vremec, C.-N. Lee, B. Phipson, W. Shi, G.K. Smyth, A.M. Lew, Y. Kato, S.N. Mueller, G.M. Davey, W.R. Heath, K. Shortman, and I. Caminschi. 2011. Targeting antigen to mouse dendritic cells via Clec9A induces potent CD4 T cell responses biased toward a follicular helper phenotype. *J Immunol*. 187:842–850.

Li, J., F. Ahmet, L.C. Sullivan, A.G. Brooks, S.J. Kent, R. De Rose, A.M. Salazar, C. Reis e Sousa, K. Shortman, M.H. Lahoud, W.R. Heath, and I. Caminschi. 2015. Antibodies targeting Clec9A promote strong humoral immunity without adjuvant in mice and non-human primates. *Eur J Immunol*. 45:854–864. doi:10.1002/eji.201445127.

Macal, M., Y. Jo, S. Dallari, A.Y. Chang, J. Dai, S. Swaminathan, E.J. Wehrens, P. Fitzgerald-Bocarsly, and E.I. Zúñiga. 2018. Self-Renewal and Toll-like Receptor Signaling Sustain Exhausted Plasmacytoid Dendritic Cells during Chronic Viral Infection. *Immunity*. 48:730-744.e5. doi:10.1016/j.immuni.2018.03.020.

Merad, M., P. Sathe, J. Helft, J. Miller, and A. Mortha. 2013. The dendritic cell lineage: ontogeny and function of dendritic cells and their subsets in the steady state and the inflamed setting. *Annu Rev Immunol*. 31:563–604.

Van Panhuys, N. 2016. TCR signal strength alters T-DC activation and interaction times and directs the outcome of differentiation. *Front Immunol*. 7. doi:10.3389/fimmu.2016.00006.

Pigni, M., D. Ashok, M. Stevanin, and H. Acha-Orbea. 2018. Establishment and Characterization of a Functionally Competent Type 2 Conventional Dendritic Cell Line. *Front Immunol*. 9:1912. doi:10.3389/fimmu.2018.01912.

Pratama, A., M. Srivastava, N.J. Williams, I. Papa, S.K. Lee, X.T. Dinh, A. Hutloff, M.A. Jordan, J.L. Zhao, R. Casellas, V. Athanasopoulos, and C.G. Vinuesa. 2015. MicroRNA-146a regulates ICOS-ICOSL signalling to limit accumulation of T follicular helper cells and germinal centres. *Nat Commun*. 6:6436.

Sage, P.T., and A.H. Sharpe. 2015. In vitro assay to sensitively measure T(FR) suppressive capacity and T(FH) stimulation of B cell responses. *Methods Mol Biol*. 1291:151–160.

bioRxiv preprint doi: https://doi.org/10.1101/2025.01.10.632426; this version posted January 14, 2025. The copyright holder for this preprint (which was not certified by peer review) is the author/funder, who has granted bioRxiv a license to display the preprint in perpetuity. It is made available under aCC-BY-ND 4.0 International license.

Sanchis, P., O. Fernández-Gayol, G. Comes, K. Aguilar, A. Escrig, M. Giralt, R.D. Palmiter, and J. Hidalgo. 2020. A new mouse model to study restoration of interleukin-6 (IL-6) expression in a Cre-dependent manner: microglial IL-6 regulation of experimental autoimmune encephalomyelitis. *J Neuroinflammation*. 17. doi:10.1186/s12974-020-01969-0.

Satpathy, A.T., W. KC, J.C. Albring, B.T. Edelson, N.M. Kretzer, D. Bhattacharya, T.L. Murphy, and K.M. Murphy. 2012. Zbtb46 expression distinguishes classical dendritic cells and their committed progenitors from other immune lineages. *Journal of Experimental Medicine*. 209:1135–1152.

Schlitzer, A., V. Sivakamasundari, J. Chen, H.R. Bin Sumatoh, J. Schreuder, J. Lum, B. Malleret, S. Zhang, A. Larbi, F. Zolezzi, L. Renia, M. Poidinger, S. Naik, E.W. Newell, P. Robson, and F. Ginhoux. 2015. Identification of cDC1- and cDC2-committed DC progenitors reveals early lineage priming at the common DC progenitor stage in the bone marrow. *Nat Immunol*. 16:718–728.

Steiner, T.M., W.R. Heath, and I. Caminschi. 2022. The unexpected contribution of conventional type 1 dendritic cells in driving antibody responses. *Eur J Immunol*. 52:189–196. doi:10.1002/eji.202149658.

Varga, G., S. Balkow, M.K. Wild, A. Stadtbaeumer, M. Krummen, T. Rothoeft, T. Higuchi, S. Beissert, K. Wethmar, K. Scharffetter-Kochanek, D. Vestweber, and S. Grabbe. 2007. Active MAC-1 (CD11b/CD18) on DCs inhibits full T-cell activation. *Blood*. 109:661–669. doi:10.1182/blood-2005-12-023044.

Wang, H., S. Jain, P. Li, J.X. Lin, J. Oh, C. Qi, Y. Gao, J. Sun, T. Sakai, Z. Naghashfar, S. Abbasi, A.L. Kovalchuk, S. Bolland, S.L. Nutt, W.J. Leonard, and H.C. Morse. 2019. Transcription factors IRF8 and PU.1 are required for follicular B cell development and BCL6-driven germinal center responses. *Proc Natl Acad Sci U S A*. 116:9511–9520. doi:10.1073/pnas.1901258116.

Watanabe, M., C. Fujihara, A.J. Radtke, Y.J. Chiang, S. Bhatia, R.N. Germain, and R.J. Hodes. 2017. Co-stimulatory function in primary germinal center responses: CD40 and B7 are required on distinct antigenpresenting cells. *Journal of Experimental Medicine*. doi:10.1084/jem.20161955.

Weber, J.P., F. Fuhrmann, R.K. Feist, A. Lahmann, M.S. Al Baz, L.-J. Gentz, D. Vu Van, H.W. Mages, C. Haftmann, R. Riedel, J.R. Grün, W. Schuh, R.A. Kroczek, A. Radbruch, M.-F. Mashreghi, and A. Hutloff. 2015. ICOS maintains the T follicular helper cell phenotype by down-regulating Krüppel-like factor 2. *J Exp Med*. 212:217–233.

Yao, C., S.M. Zurawski, E.S. Jarrett, B. Chicoine, J. Crabtree, E.J. Peterson, G. Zurawski, D.H. Kaplan, and B.Z. Igyártó. 2015. Skin dendritic cells induce follicular helper T cells and protective humoral immune responses. *Journal of Allergy and Clinical Immunology*. 136:1387-1397.e7. doi:10.1016/j.jaci.2015.04.001.

Yin, X., S. Chen, and S.C. Eisenbarth. 2021. Dendritic Cell Regulation of T Helper Cells. *Annu Rev Immunol*. 39:759–790. doi:10.1146/annurev-immunol-101819-025146.

bioRxiv preprint doi: https://doi.org/10.1101/2023.01.10.032420; this version posted January 14, 2023. The copyright holder for this preprint (which was not certified by peer review) is the author/funder, who has granted bioRxiv a license to display the preprint in perpetuity. It is made available under aCC-BY-ND 4.0 International license.

Fig. 1.

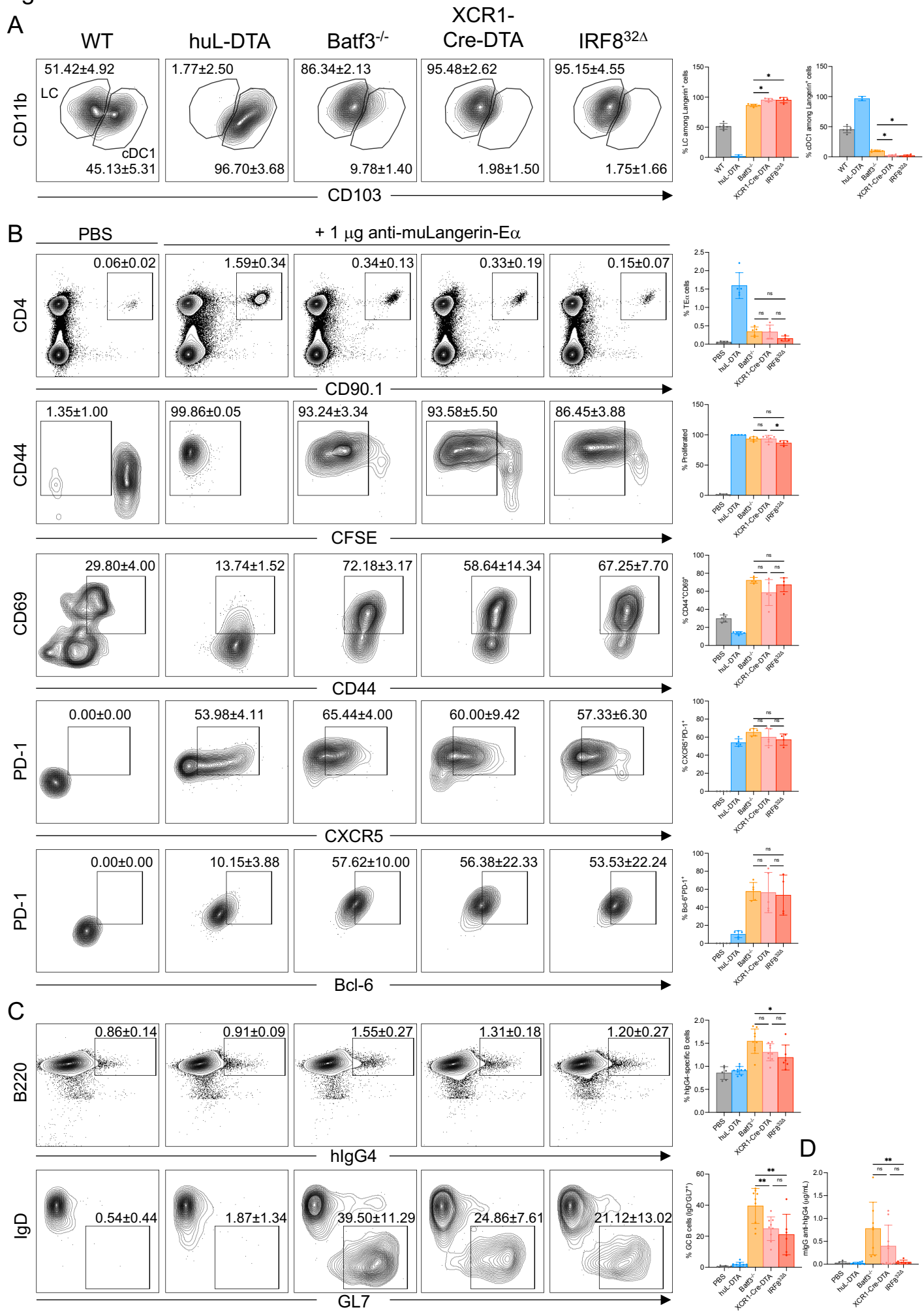

(which was not certified by peer review) is the author/funder, who has granted bioRxiv a license to display the preprint in perpetuity. It is m
available under aCC-BY-ND 4.0 International license.

Fig. 2

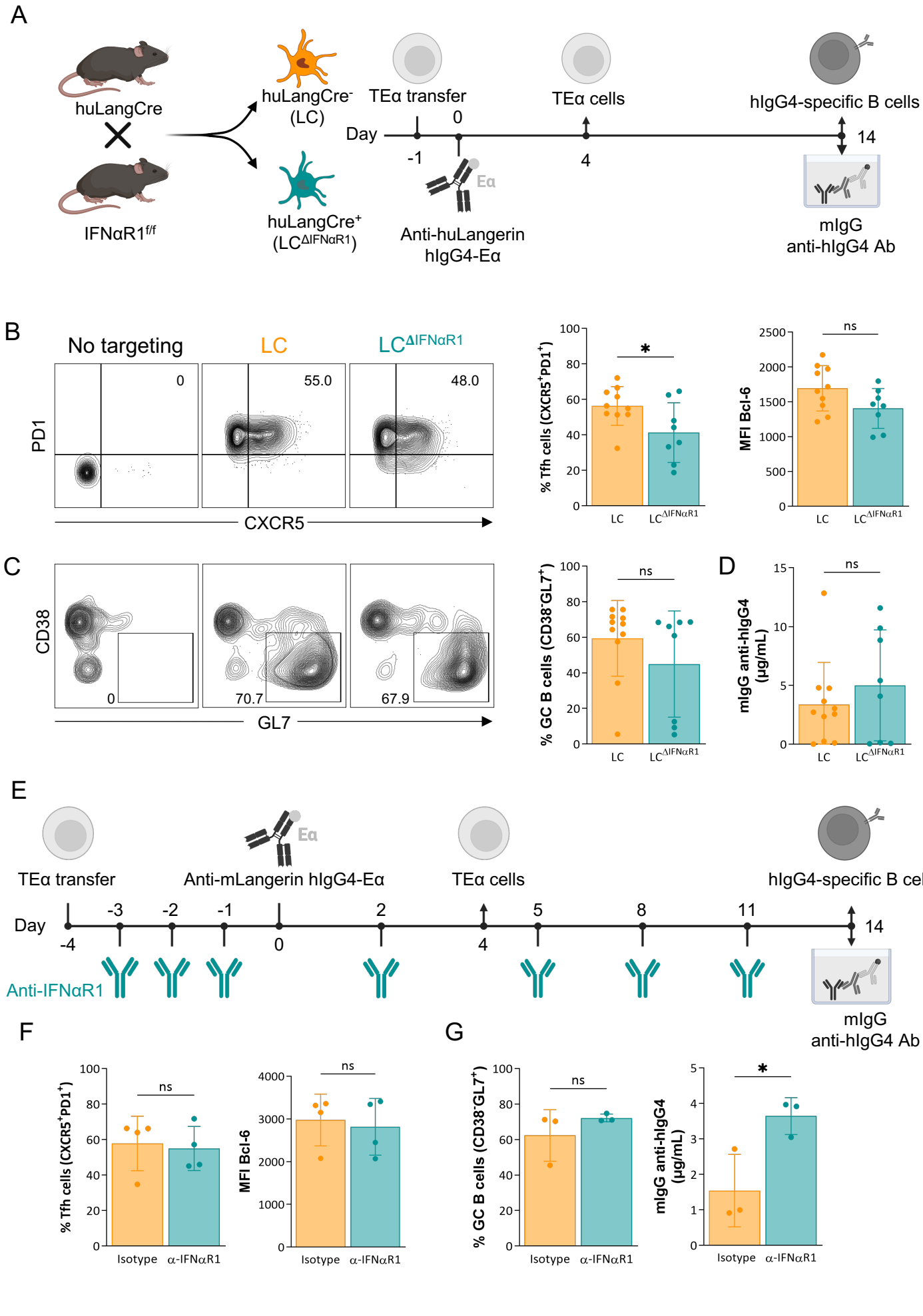

(which was not certified by peer review) is the author/funder, who has granted bioRxiv a license to display the preprint in perpetuity. It is m
available under aCC-BY-ND 4.0 International license.

Fig. 3

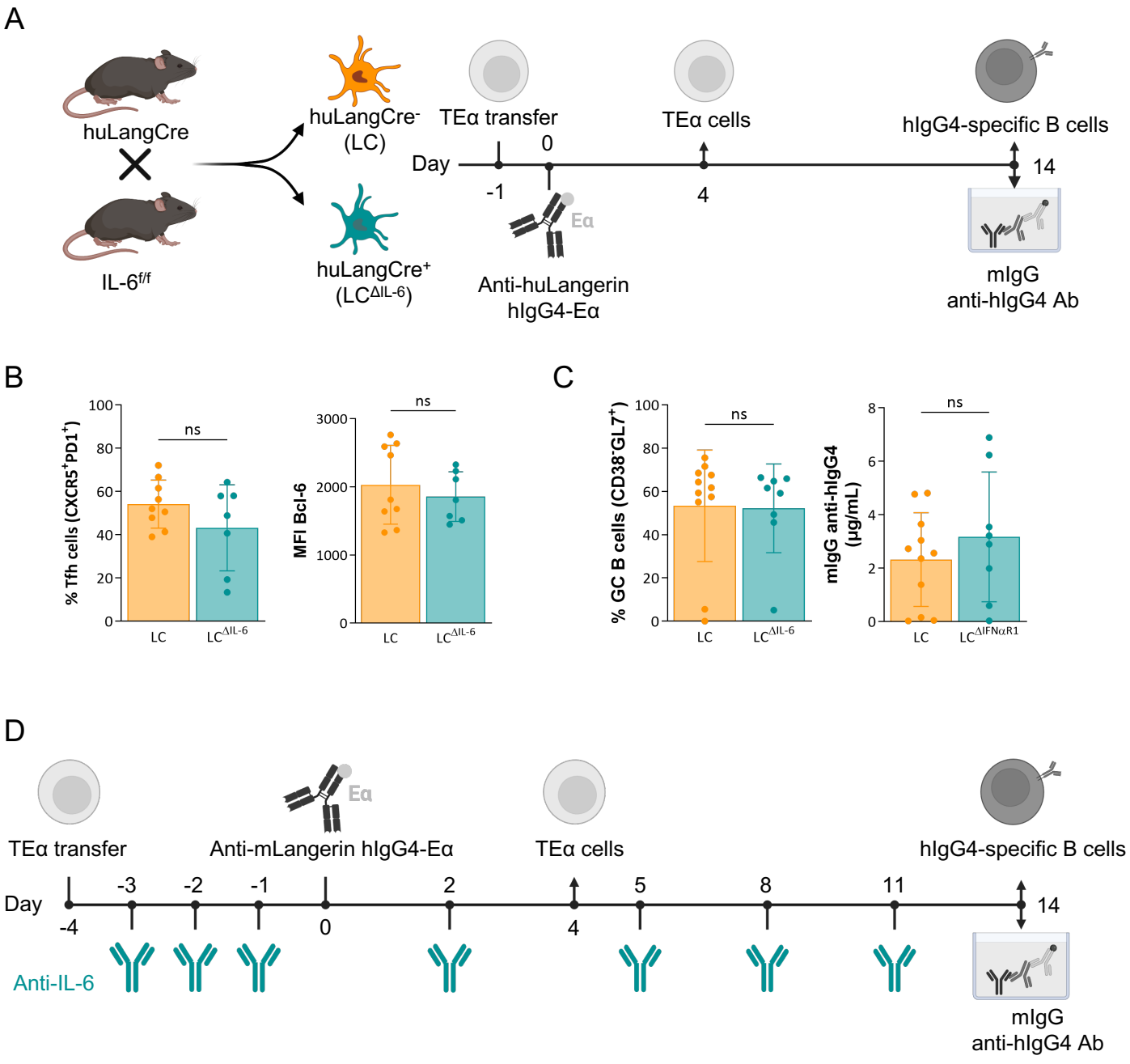

(which was not certified by peer review) is the author/funder, who has granted bioRxiv a license to display the preprint in perpetuity. It is m
available under aCC-BY-ND 4.0 International license.

Fig. 4

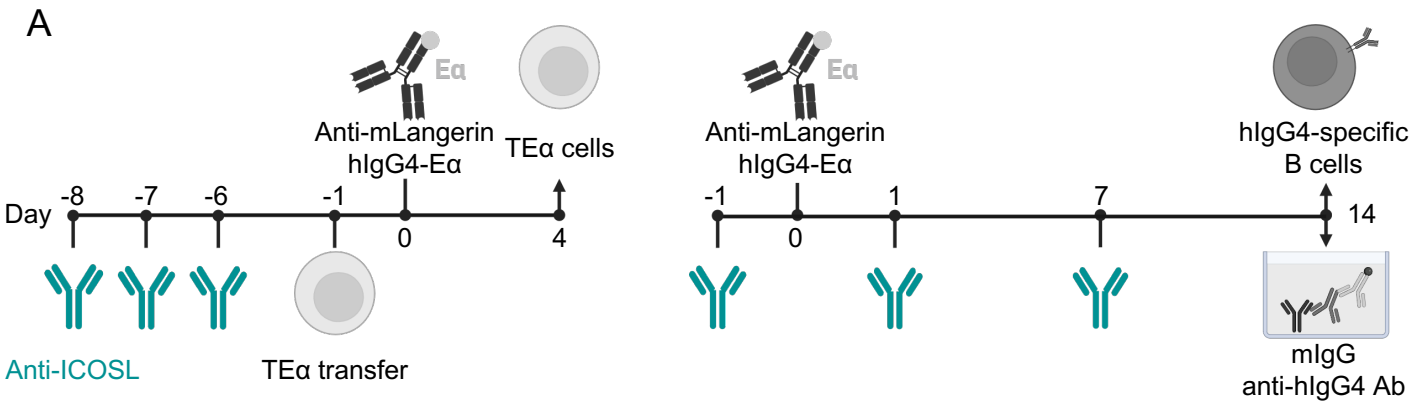

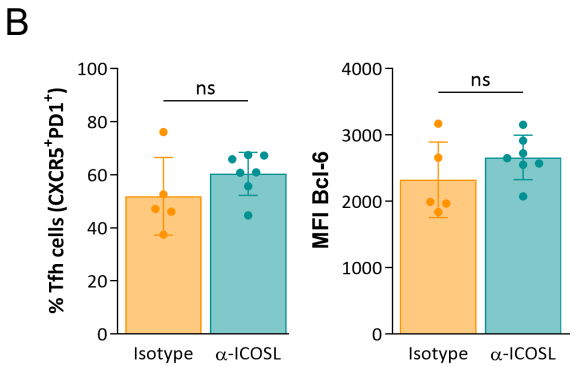

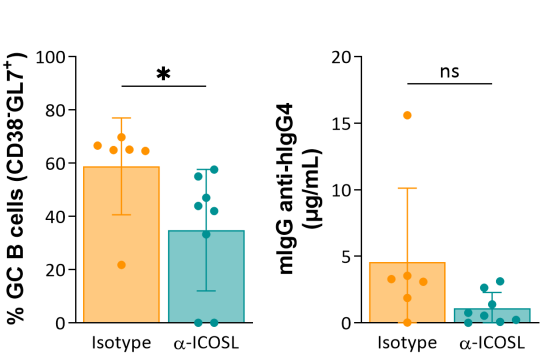

(which was not certified by peer review) is the author/funder, who has granted bioRxiv a license to display the preprint in perpetuity. It is m
available under aCC-BY-ND 4.0 International license.
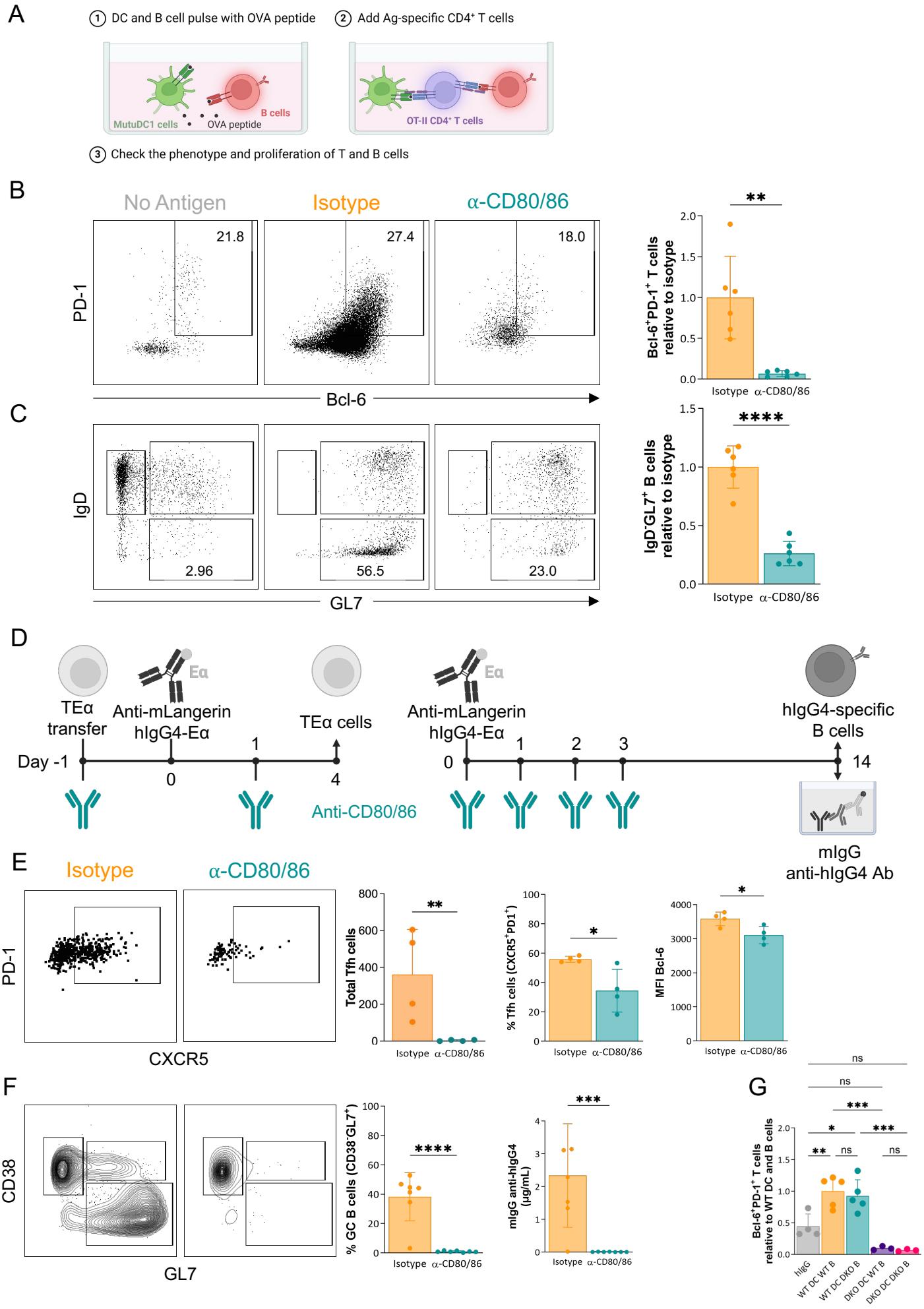
Fig. 5